Original Article

The morphology of angle dysgenesis assessed by ultrasound biomicroscopy and its relationship with glaucoma severity and mutant genes in Axenfeld-Rieger syndrome

Qingdan Xu[1], Youjia Zhang[1], Li Wang[1,2,3], Xueli Chen[1,2,3], Xinghuai Sun[1,2,3,4], Yuhong Chen[1,2,3]

[1]Department of Ophthalmology, Eye, Ear, Nose, and Throat Hospital, Fudan University, Shanghai, China; [2]NHC Key Laboratory of Myopia, Chinese Academy of Medical Sciences, Fudan University, Shanghai, China; [3]Shanghai Key Laboratory of Visual Impairment and Restoration, Fudan University, Shanghai, China; [4]State Key Laboratory of Medical Neurobiology, Institutes of Brain Science, Fudan University, Shanghai, China

Contributions: (I) Conception and design: X Sun, Y Chen; (II) Administrative support: X Sun, Y Chen; (III) Provision of study materials or patients: All authors; (IV) Collection and assembly of data: L Wang, X Chen; (V) Data analysis and interpretation: Q Xu, Y Zhang; (VI) Manuscript writing: All authors; (VII) Final approval of manuscript: All authors.

Correspondence to: Yuhong Chen, MD, PhD. Department of Ophthalmology, Eye, Ear, Nose, and Throat Hospital, Fudan University, 83 Fenyang Road, Shanghai 200031, China; NHC Key Laboratory of Myopia, Chinese Academy of Medical Sciences, Fudan University, Shanghai, China; Shanghai Key Laboratory of Visual Impairment and Restoration, Fudan University, Shanghai, China. Email: yuhongchen@fudan.edu.cn; Xinghuai Sun, MD, PhD. Department of Ophthalmology, Eye, Ear, Nose, and Throat Hospital, Fudan University, 83 Fenyang Road, Shanghai 200031, China; NHC Key Laboratory of Myopia, Chinese Academy of Medical Sciences, Fudan University, Shanghai, China; Shanghai Key Laboratory of Visual Impairment and Restoration, Fudan University, Shanghai, China; State Key Laboratory of Medical Neurobiology, Institutes of Brain Science, Fudan University, Shanghai, China. Email: xhsun@shmu.edu.cn.

Background: Axenfeld-Rieger syndrome (ARS), a developmental disorder, involves anterior segment abnormalities and can lead to glaucoma. However, limited research has addressed the ultrasound biomicroscopy (UBM) characteristics of ARS. This study aimed to assess the anterior chamber angle features using UBM in ARS and determine their correlation with glaucoma severity and mutant genes.

Methods: UBM examination was conducted for 42 patients diagnosed with ARS and glaucoma. The morphology of the anterior chamber angle was classified into 6 types (type A, pure high iris insertion; type B, posterior embryotoxon; type C, iris process; type D, trabecular-iris synechia; type E, peripheral iridocorneal adhesion; type F, goniodysgenesis). Candidate genes were sequenced with next-generation sequencing. Correlations of clinical characteristics with angle dysgenesis types and mutant genes were analyzed.

Results: Among the 42 patients recruited, 6 eyes were excluded for poor quality UBM images or lack of glaucoma development. The remaining 78 eyes were categorized into 6 groups according to their dominant type of anterior chamber angle (>2 quadrants). There were statistically significant differences in onset age of glaucoma (P<0.001), untreated intraocular pressure (IOP) (P=0.016), vertical cup to disc ratio (P=0.001), and age at surgery (P<0.001) among the groups. Eyes in the type C and D groups developed glaucoma and underwent surgery at an earlier age, while eyes in the type B, E, and F groups developed glaucoma at a relatively later age. Eyes in type A group developed glaucoma and underwent surgery at the latest age, and had the lowest untreated IOP compared to the other groups. Patients with *FOXC1* defects were more likely to have angle type B, type C, and type D (accounting for 93.8% of the total), whereas patients with *PITX2* defects were more likely to have angle type A, type E, and type F (accounting for 92.1% of the total).

Conclusions: UBM is powerful for evaluating the anterior segment abnormalities in ARS. Combined with genetic testing results, the morphological classification helps to assess the severity of glaucoma.

Keywords: Anterior chamber angle; Axenfeld-Rieger syndrome (ARS); glaucoma severity; mutant gene; ultrasound biomicroscopy (UBM)

Submitted Mar 17, 2023. Accepted for publication Aug 14, 2023. Published online Sep 11, 2023.
doi: 10.21037/qims-23-348
View this article at: https://dx.doi.org/10.21037/qims-23-348

Introduction

Axenfeld-Rieger syndrome (ARS) is characterized by developmental abnormalities involving multiple systems and organs, mainly affecting ocular anterior segment (1). It originates from abnormal migration of neural crest cells, causing the developmental defects of iridocorneal angle and aqueous humor outflow structures (2,3). Patients are at 50% risk of developing glaucoma, which can result in optic nerve damage and irreversible loss of the visual field (4,5). ARS is genetically heterogeneous, and 40–63% of patients have genetic defects in 2 developmental transcription factor genes: *FOXC1* (the forkhead box C1 gene) or *PITX2* (the pituitary homeobox 2 gene) (6-11).

Previous reports have described the anomalous anterior segment of ARS, which may include posterior embryotoxon, iridocorneal adhesions, iris hypoplasia, incomplete angle recession, trabecular meshwork atrophy, and Schlemm's canal occlusion (1,5,12,13). However, due to the opacity of the cornea or young age of some patients, it is often difficult to clearly observe the chamber angle structure by means of slit lamp or gonioscopy.

Ultrasound biomicroscopy (UBM) is an ultrasound technique which provides noninvasive and dynamic high-resolution imaging of the anterior ocular segment *in vivo* (14). It is particularly important for patients with opaque cornea (15) and useful in visualizing the structures behind the iris (16,17). Thus far, a few studies have depicted the characteristics of anterior segment structure in ARS using UBM (10,18-20); however, no report has evaluated and classified the iridocorneal angle morphology of ARS in detail. Our study therefore aimed to assess the morphology of chamber angle in ARS and to determine the correlation of anterior chamber angle morphology with glaucoma severity and mutant genes. We present this article in accordance with the STROBE reporting checklist (available at https://qims.amegroups.com/article/view/10.21037/qims-23-348/rc).

Methods

Patients

We consecutively recruited 42 patients diagnosed with ARS and glaucoma simultaneously between April 2000 and December 2021 in Eye, Ear, Nose, and Throat Hospital of Fudan University. Our cohort was a mixture of familial and isolated cases of ARS, including 4 familial cases and 38 isolated cases. Patients were followed up for a median duration of 79 (IQR, 38–128) months. This study was approved by the Institutional Review Board of Eye, Ear, Nose, and Throat Hospital of Fudan University (No. KJ2011-04) and followed the tenets of the Declaration of Helsinki (as revised in 2013). Written consent forms were obtained from all patients or their legal guardians. The criteria for inclusion were as follows: (I) congenital ocular abnormalities, including malformations of the anterior chamber angle, posterior embryotoxon, iridocorneal adhesions traversing the anterior chamber, iris hypoplasia, polycoria, and corectopia; and (II) with or without systemic abnormalities, including craniofacial abnormalities, dental anomalies, redundant periumbilical skin, and other systemic manifestations (21,22). Eyes with prior histories of trauma, surgeries, or uveitis were excluded. Diagnosis of glaucoma in adults was based on at least 2 of the following clinical features: intraocular pressure (IOP) >21 mmHg, glaucomatous optic disc damage (cup to disc ratio of >0.5 or inter-eye asymmetry of >0.2, neuroretinal rim thinning, notching, disc hemorrhage, etc.), or glaucomatous visual field defects (4). According to Childhood Glaucoma Research Network criteria, childhood glaucoma was diagnosed if at least 2 of the following features were present: (I) IOP >21 mmHg; (II) glaucomatous optic neuropathy (progressively increased cup to disc ratio; cup to disc ratio asymmetry of ≥0.2 in similar-sized optic discs; and thinning of the focal rim); (III) progressive myopia or myopic shift with increased ocular dimensions exceeding normal growth; (IV) reproducible visual field defect with no other possible causes; (V) or corneal findings including Haab's striae, corneal edema, corneal diameter >11 mm in a neonate, >12 mm in a child under 1 year old, or >13 mm at any age (23).

Clinical investigation

Of all participants, detailed medical histories were collected, including ocular and systemic medication, family

history, history of trauma, and surgeries. Comprehensive ophthalmologic examinations were conducted, including visual acuity examination, ophthalmoscopy, slit-lamp biomicroscopy, gonioscopy, IOP measurement using Goldmann applanation tonometer or Tono-Pen (Reichert Technologies, Depew, NY, USA), anterior segment photography, color fundus photography, B-mode ultrasonography, and A-mode ultrasonography. Adults and cooperative children underwent visual field examinations with the Octopus 101 (Haag-Streit, Inc., Köniz, Switzerland) or Humphrey Visual Field Analyzer 750 (Zeiss-Humphrey Systems, Dublin, CA, USA).

The following information was recorded and analyzed for each eye: onset age of glaucoma, untreated IOP, vertical cup to disc ratio (VCDR), corneal clarity, age at surgery, type of surgery, and the surgical outcome. Corneal clarity was scored as follows: 1, corneal transparence; 2, mild corneal opacity with visible iris; 3, severe corneal opacity with invisible iris; and 4, severe corneal opacity with neovascularization. An addition of 0.5 was included if there were Haab's striae (24). Surgical failure was defined as a postoperative IOP >21 mmHg with the necessity of additional antiglaucoma medications or secondary surgical therapy.

UBM examination

UBM (MD-300L; MEDA Co., Tianjin, China) with a 50-MHz resolution was performed for all the patients before surgeries. The UBM examinations were conducted by experienced technicians in Eye, Ear, Nose, and Throat Hospital of Fudan University following the same operating procedure. Patients were placed in the supine position, and a water bath in contact with the eye was applied to examine the anterior segment. Patients older than 10 years old underwent UBM examination under topical anesthesia, while those younger than 10 years old underwent general anesthesia. The morphology of the iridocorneal angle was classified into 6 types: type A, pure high insertion of the iris root with or without abnormal tissue membrane covering the anterior chamber angle (*Figure 1A*); type B, posterior embryotoxon, shown as hyperechoic foci on the posterior corneal surface, essentially indicating a prominent and anteriorly displaced Schwalbe's line (*Figure 1B*); type C, iris process, indicated as abnormal strands of the peripheral iris extending toward the protruding Schwalbe's line (*Figure 1C*); type D, trabecular-iris synechia corresponding to the anterior synechia of the iris root on the trabecular meshwork without anterior chamber angle recess (*Figure 1D*); type E, peripheral iridocorneal adhesion involving anterior displacement of the iris and iridocorneal adhesion (*Figure 1E*); type F, goniodysgenesis, characterized by loss of normal chamber angle configuration with indistinguishable scleral spur and deep posterior chamber (*Figure 1F*). The anterior chamber angle was scanned for the inferior, temporal, superior, and nasal quadrants. Two scans in each quadrant per eye were conducted and each scan was recorded as a 0.5 quadrant for analysis. The UBM images were evaluated by 2 investigators who were blinded to the clinical details and genetic testing results. Eyes exhibiting prominence of a specific type of the iridocorneal angle morphology were categorized into the corresponding groups. The ciliary body on UBM images was also evaluated. Ciliary body hypoplasia was defined as a short and thin ciliary body with unclear anatomical characteristics.

Genetics analysis

Candidate genes were sequenced in all patients with next-generation sequencing using the Illumina Miseq platform (Illumina, San Diego, CA, USA) with the 2×300 bp paired-end read module. The panel covered 289 genes associated with anterior segment dysgenesis and glaucoma. The average coverage depth was 100 times, and 90% of targeted bases were covered 40 times or more. All detected variants and the segregation on all available family members were verified through Sanger sequencing.

Statistical analysis

All data were analyzed using SPSS version 20.0 (IBM Corp., Armonk, NY, USA) and GraphPad Prism software version 9.0 (GraphPad Software, San Diego, CA, USA). Onset age of glaucoma and age at surgery with nonnormal distributions were evaluated using the Kruskal-Wallis test with Dunn post hoc test. Comparisons of sex, surgical rate, type of surgery, surgical failure rate, and anterior chamber angle type among patients with different mutant genes were assessed using Pearson chi-squared test or Fisher exact test with Bonferroni post hoc test. To adjust for the correlation between 2 eyes of patients with both eyes included in the analysis, generalized estimating equations were used to compare the onset age of glaucoma, untreated IOP, VCDR, corneal clarity score, and age at surgery. A generalized linear mixed model was employed to compare the surgical

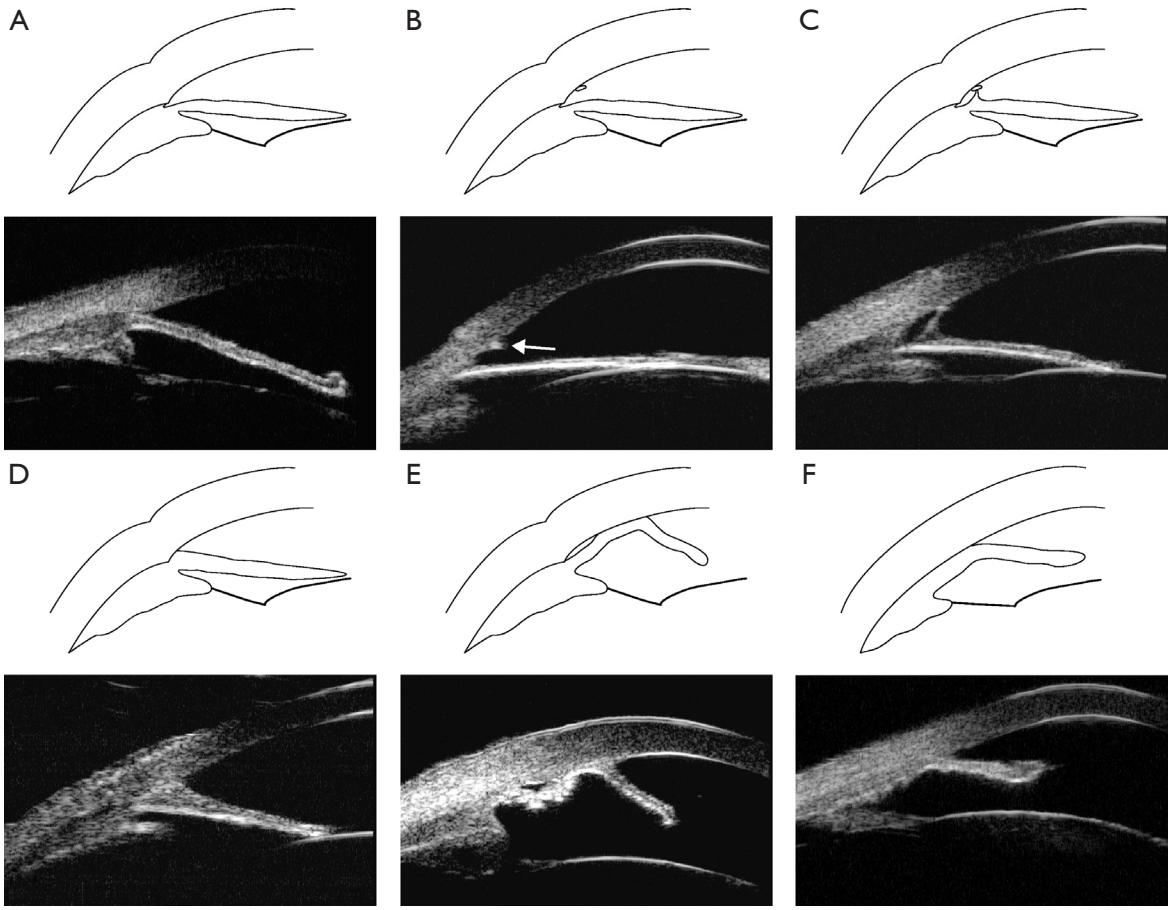

Figure 1 Morphology of the iridocorneal angle was classified into 6 types. (A) Type A, pure high insertion of the iris root with or without abnormal tissue membrane covering the anterior chamber angle. (B) Type B, posterior embryotoxon, shown as hyperechoic foci (white arrow) on the posterior corneal surface. (C) Type C, iris process, indicated as abnormal strands of peripheral iris extending to the protruding Schwalbe's line. (D) Type D, trabecular-iris synechia corresponding to the anterior synechia of the iris root onto the trabecular meshwork without anterior chamber angle recess. (E) Type E, peripheral iridocorneal adhesion involving anterior displacement of the iris and iridocorneal adhesion. (F) Type F, goniodysgenesis, characterized by the loss of a normal chamber angle configuration with indistinguishable scleral spur and a deep posterior chamber.

rate, type of surgery, surgical failure rate, and proportion of the ciliary body hypoplasia among the 6 groups of eyes. Statistical significance was set at $P<0.05$.

Results

Demographic characteristics

In total, 42 patients were enrolled in this study. Among them, 26 were male (61.9%) and 16 were female (38.1%). Of the 42 patients with glaucoma, 39 cases were bilateral and 3 cases were unilateral. The onset age of glaucoma ranged from 0 to 70 years, with 10 patients (10/42, 23.8%) and 19 eyes (19/81, 23.5%) developing glaucoma in infancy (0–1 year), 16 patients (16/42, 38.1%) and 30 eyes (30/81, 37.0%) in adolescence (1–18 years), 11 patients (11/42, 26.2%) and 22 eyes (22/81, 27.2%) in young adulthood (18–40 years), and 5 patients (5/42, 11.9%) and 10 eyes (10/81, 12.3%) after middle age (>40 years). In all patients with both eyes diagnosed with glaucoma, the interval of occurrence of glaucoma between the 2 eyes was less than 1 year.

Clinical characteristics

The UBM images of all 42 participants were obtained. Of

Table 1 Comparison of clinical characteristics among the 6 groups of eyes

Characteristic	Type A group	Type B group	Type C group	Type D group	Type E group	Type F group	P
Eyes	14 (17.9)	22 (28.2)	9 (11.5)	5 (6.4)	20 (25.6)	8 (10.3)	–
Onset age of glaucoma (year)	32.0 [18.0–70.0]	15.0 [0.0–42.0]	0.3 [0.0–14.0]	0.1 [0.0–15.0]	13.5 [0.4–46.0]	19.5 [16.0–36.0]	<0.001*
Untreated IOP (mmHg)	24.4 [12.0–48.0]	38.5 [19.0–72.0]	33.0 [21.0–38.0]	40.0 [34.0–46.0]	39.0 [23.0–60.0]	39.6 [21.9–54.5]	0.016*
VCDR	0.90 [0.35–1.00]	0.95 [0.40–1.00]	0.95 [0.30–1.00]	0.95 [0.90–1.00]	0.90 [0.40–1.00]	1.00 [0.90–1.00]	0.001*
Corneal clarity score	1 [1–2]	1 [1–3]	1 [1–2.5]	2 [1–2]	1 [1–2.5]	1 [1–2]	0.146
Surgical rate	4 (28.6)	16 (72.7)	7 (77.8)	5 (100.0)	15 (75.0)	8 (100.0)	0.086
Age at surgery (year)	38.5 [34.0–71.0]	10.5 [0.1–52.0]	0.8 [0.2–15.0]	0.3 [0.2–15.0]	24.0 [0.8–51.0]	22.5 [16.0–36.0]	<0.001*
Type of surgery (trabeculotomy/ filtering surgery)	0/4	6/10	5/2	3/2	2/13	0/8	0.001*
Surgical failures within 5 years	2 (50.0)	1 (6.3)	0 (0.0)	1 (20.0)	6 (40.0)	2 (25.0)	0.408

Data are presented as n (%) or median [range]. Type A: pure high iris insertion; Type B: posterior embryotoxon; Type C: iris process; Type D: trabecular-iris synechia; Type E: peripheral iridocorneal adhesion; Type F: goniodysgenesis. Eyes were categorized into 6 groups according to their dominant types of anterior chamber angle (>2 quadrants of the angle). Asterisk (*) indicates statistical significance (P<0.05). IOP, intraocular pressure; VCDR, vertical cup to disc ratio.

the 84 eyes, 3 were excluded for poor quality images and another 3 were excluded for lack of glaucoma development. In all of the remaining 78 eyes, different degrees of iris atrophy with high insertion of the iris root were present. Ciliary body hypoplasia was observed in 45 eyes (45/78, 57.7%). The iridocorneal angle morphology of each patient is shown in Table S1. Moreover, 57 eyes (57/78, 73.1%) had at least 2 types of angle morphology, whereas 21 eyes (21/78, 26.9%) had an identical type of anterior chamber angle in the 4 quadrants. By number of quadrants, type B (89.5/312, 28.7%) was the most common type, while type D was the rarest one (18/312, 5.8%).

The 78 eyes with UBM examinations in our study were categorized as type A group (n=14), type B group (n=22), type C group (n=9), type D group (n=5), type E group (n=20), and type F group (n=8) according to their dominant types of anterior chamber angle (>2 quadrants of the angle). Both eyes were categorized into the same group in all patients with bilateral UBM images. The clinical characteristics and comparison analysis among the 6 groups are shown in *Table 1*. There were statistically significant differences in onset age of glaucoma (P<0.001) and age at surgery (P<0.001) between the groups. Eyes in type C and D groups developed glaucoma and underwent surgery at an earlier age, with the median being less than 1 year of age; eyes in the type B, E, and F groups developed glaucoma and underwent surgery at a relatively later age, with medians of 10 to 25 years of age; eyes in the type A group developed glaucoma and underwent surgery at a later age, with the median being more than 30 years of age. Eyes in type A group had the lowest untreated IOP, with a median of 24.4 mmHg, while the other groups all had medians greater than 30.0 mmHg (P=0.016). The VCDR was significantly larger in type D and F groups than in the other groups (P=0.001). Furthermore, the type A group had the lowest surgical rate (28.6%) compared to the others (from 70% to 100%), with a marginal P value (P=0.086). The corneal clarity scores and surgical failure rate within 5 years were not statistically significantly different among the 6 groups. We also compared the proportions of the ciliary body hypoplasia among different groups of eyes and found that eyes in the type F group had the highest proportion (8/8, 100.0%), eyes in the type A group (10/14, 71.4%) and type E group (13/20, 65.0%) had a relatively higher proportion, eyes in the type B group (10/22, 45.5%) and type D group (2/5, 40.0%) had a relatively lower proportion, and eyes in type C group had the lowest proportion (2/9, 22.2%). These differences were statistically significant (P=0.017).

Genetic defect and dysgenesis of the iridocorneal angle

A total of 15 patients were detected as carrying *FOXC1*

Table 2 Comparison of clinical characteristics among patients with different mutant genes

Characteristic	*FOXC1*	*PITX2*	Negative	P
Patients	15 (35.7)	14 (33.3)	13 (31.0)	–
Sex (male/female)	10/5	8/6	8/5	0.870
Onset age of glaucoma (year)*†	0.3 [0.0–24.0]	21.0 [0.4–61.0]	22.0 [10.0–70.0]	<0.001
Untreated IOP (mmHg)	37.0 [20.0–72.0]	34.8 [20.0–60.0]	34.0 [12.0–54.5]	0.878
VCDR	0.95 [0.30–1.00]	0.90 [0.40–1.00]	0.90 [0.35–1.00]	0.926
Corneal clarity score*†	2 [1–3]	1 [1–2.5]	1 [1–2]	0.009
Surgical rate	12 (80.0)	10 (71.4)	9 (69.2)	0.826
Age at surgery (year)*†	0.6 [0.1–15.0]	29.5 [0.8–71.0]	19.0 [11.0–52.0]	0.001
Type of surgery (trabeculotomy/filtering surgery)*†	8/4	1/9	0/9	0.001
Surgical failures within 5 years*	1 (8.3)	6 (60.0)	3 (33.3)	0.041

Data are presented as n (%) or median [range]. *, statistically significant difference between patients with *FOXC1* defects and *PITX2* defects (P<0.05). †, statistically significant difference between patients with *FOXC1* defects and without defects in 2 genes (P<0.005). IOP, intraocular pressure; VCDR, vertical cup to disc ratio.

defects, 14 patients were detected as carrying *PITX2* defects, and 13 patients showed no defects in any candidate genes (Table S1). All detected variants were heterozygous and predicted to be pathogenic (8). As shown in *Table 2*, there was no statistically significant difference in sex (P=0.870) among the patients with *FOXC1* defects, patients with *PITX2* defects, and patients without defects in the 2 genes. The patients with *FOXC1* defects were more likely to have an earlier onset age of glaucoma than were patients with *PITX2* defects (P=0.007) and those without defects in the 2 genes (P=0.001). There was no significant difference in untreated IOP (P=0.878) or VCDR (P=0.926) among the 3 groups. With respect to the corneal clarity, patients with *FOXC1* defects had higher scores than did patients with *PITX2* defects (P=0.036) and those without defects in the 2 genes (P=0.002). Although no significant difference was found in the surgical rate (P=0.826), the patients with *FOXC1* defects underwent surgery at a statistically significantly younger age than did patients with *PITX2* defects (P=0.002) and those without defects in the 2 genes (P=0.004). No statistically significant difference in onset age of glaucoma, corneal clarity, or age at surgery was observed between patients with *PITX2* defects and those without defects in the 2 genes. During the follow-up, we found that the patients with *FOXC1* defects had a lower rate of surgical failure within 5 years than did patients with *PITX2* defects (P=0.020).

With regard to the anterior chamber angle dysgenesis, patients with *FOXC1* defects had angle type B, type C, and type D more frequently compared to patients with *PITX2* defects, whereas patients with *PITX2* defects had angle type A, type E, and type F more frequently compared to patients with *FOXC1* defects. Comparison of angle dysgenesis types of the different mutant genes is presented in *Table 3* and *Figure 2*.

Discussion

UBM is a valuable and reliable technique, which provides high-resolution images similar to a microscope (25). It contributes to the evaluation of anterior segment structure, especially for those not easily accessible by conventional clinical examination underneath a turbid cornea (20,26). Moreover, compared with anterior segment optical coherence tomography, UBM can visualize and evaluate the structures of the ciliary body and therefore is the best tool for patients with anterior segment dysgenesis who often have iris anterior adhesions (16,17,27).

Based on the reported studies, the pathogenesis of ARS involves the developmental arrest of structures derived from neural crest cells in the third trimester of pregnancy resulting in the retention of endothelial layer on the iridocorneal angle and iris, together with the incomplete posterior sliding of uveal tissue (5). Contraction of the retained strands leads to the abnormalities of anterior

Table 3 Angle dysgenesis types in patients with different mutant genes

Mutant gene	Affected individuals	Eyes examined	Total quadrants	Anterior chamber angle type, n (%)					
				Type A*†	Type B*†‡	Type C*†‡	Type D*†	Type E*†‡	Type F*†
FOXC1	15	28	112	6.5 (5.8)	58 (51.8)	30 (26.8)	17 (15.2)	0.5 (0.4)	0 (0)
PITX2	14	27	108	26 (24.1)	6.5 (6.0)	1.5 (1.4)	0.5 (0.5)	58.5 (54.2)	15 (13.9)
Negative	13	23	92	21.5 (23.4)	25 (27.2)	12.5 (13.6)	0.5 (0.5)	11.5 (12.5)	21 (22.8)

*, Statistically significant difference between patients with *FOXC1* defects and *PITX2* defects (P<0.001). †, Statistically significant difference between patients with *FOXC1* defects and without defects (P<0.03). ‡, Statistically significant difference between patients with *PITX2* defects and without defects (P<0.001).

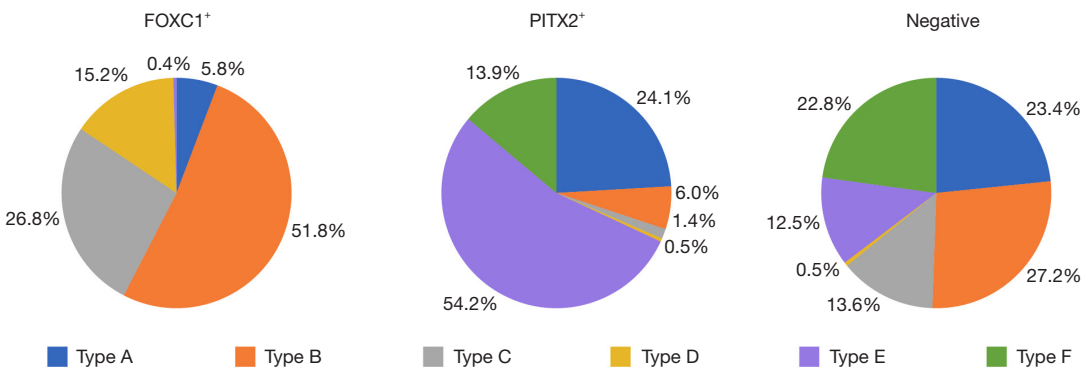

Figure 2 Pie chart of the morphological angle type for patients with different mutant genes. Each pie chart corresponds to a group of patients and depicts the frequency distribution of 6 types of anterior chamber angle: Type A, pure high iris insertion; Type B, posterior embryotoxon; Type C, iris process; Type D, trabecular-iris synechia; Type E, peripheral iridocorneal adhesion; and Type F, goniodysgenesis.

chamber (5). Previous studies have described the angle features of ARS as the peripheral iris extending toward a prominently and centrally displaced Schwalbe's line, with the thickness varying from thin to thick. The presence of an anterior iris root insertion, along with a rudimentary Schlemm's canal, can impair the outflow of aqueous humor and consequently contribute to the onset or progression of glaucoma (28,29). In this study, we considered 6 types of iridocorneal angle morphology of ARS. High insertion of the peripheral iris was observed in all eyes, which has also been reported by others as being a potential risk factor for glaucoma (5,21). Other abnormalities, including prominent Schwalbe's line in type B, iris process in type C, trabecular-iris synechia in type D, and peripheral iridocorneal adhesion in type E, although different in morphology, all originate from the deposition and contraction of the basement membrane by the primordial endothelial layer. Furthermore, UBM demonstrated ciliary body hypoplasia in 57.7% eyes, suggesting that the developmental defect in ARS involves not only the anterior chamber angle and iris but also the ciliary body. The type A angle morphology of ARS in our study shared similarities with the ultrasound biomicroscopic features reported in primary congenital glaucoma (PCG), which also arises from the hindered posterior sliding of uveal tissue. These shared features include a thin iris, small ciliary body, abnormal tissue membrane, anterior iris insertion, and absence of Schlemm's canal (30,31), thus constituting evidence supporting the phenotypic overlap between ARS and PCG.

In this study, eyes in the type A group had a lower untreated IOP and surgical rate and developed glaucoma and underwent glaucoma surgery at a relatively later age than did the eyes in the type B, C, D, and E groups, indicating that the presence of posterior embryotoxon or iridocorneal adhesions may aggravate the development of glaucoma. Previous studies have demonstrated that the pathogenetic mechanism of glaucoma in ARS is the obstruction of aqueous outflow due to a rudimentary or absent Schlemm's canal and the compact trabecular meshwork caused by developmental failure of the

intertrabecular spaces (5,32). Thus, we speculate that a larger extent of the posterior embryotoxon and iridocorneal adhesions may be a sign of the poorer chamber angle development and, as a result, predispose eyes to a greater risk of development of glaucoma in ARS. Furthermore, we found that eyes in the type E group, despite having severe iridocorneal adhesions, developed glaucoma and underwent surgery at a later age than did those in the type C and D groups with mild iridocorneal adhesions. This suggests that the extent of iridocorneal adhesions did not correlate with the severity of glaucoma, which is consistent with previous studies (3). It seems that the severity of glaucoma may be correlated with the degree of health in the remaining unclosed angles. Furthermore, since the IOP balance was simultaneously influenced by the secretion and drainage of aqueous humor, this phenomenon might also be explained by the different degrees of hypoplasia of ciliary body in ARS, which was observed in more than half of our patients and was also highly common in other anterior segment dysgenesis diseases. Notably, we examined a special morphology of chamber angle maldevelopment (type F) in this study, which was characterized by the absence of observable angle structures under gonioscopy. We found that eyes having angle type F in all quadrants developed glaucoma in adolescence (16–22 years) instead of infancy, leaving the question of aqueous humor drainage pathway unclear.

In a previous study, we reported that patients with *FOXC1* defects tended to be diagnosed with ARS at a younger age than did those with *PITX2* defects (8). Here, we further compared other clinical characteristics between *FOXC1*-defect carriers and *PITX2*-defect carriers and found that *FOXC1*-defect carriers had poorer corneal transparency and developed glaucoma and underwent surgery at a significantly younger age than did *PITX2*-defect carriers. However, *PITX2*-defect carriers had a worse surgical prognosis than did *FOXC1*-defect carriers although this is consistent with a previous study (4). Since *PITX2*-defect carriers tended to have extensive iridocorneal adhesion and a relatively older age at onset, we performed glaucoma filtering surgery (trabeculectomy and drainage implant) on most patients (9/10, 90.0%) with the *PITX2* defect. Meanwhile, we performed trabeculotomy on most patients (8/12, 66.7%) with the *FOXC1* defect. Therefore, the difference of surgical failure rates between these 2 groups of patients was possibly associated with the difference in the type of surgery. In addition, we found there to be a certain correlation between the type of the iridocorneal angle morphology and the mutant genes. *FOXC1*-defect carriers tended to have posterior embryotoxon, iris process, and trabecular-iris synechia (type B, type C, and type D), whereas *PITX2*-defect carriers usually had pure high iris insertion, peripheral iridocorneal adhesion, and goniodysgenesis (type A, type E, and type F). This suggests that the developmental alterations leading to the chamber angle changes are not precisely the same between the 2 mutant genes, which may correlate with the difference in the function of the 2 genes and their involvement in eye development.

The majority of eyes with ARS require multiple surgeries to achieve long-term IOP control (33). In our study, we followed up the patients and observed a surgical success rate without additional antiglaucoma medication of 78.2% (43/55) at 5 years. Specifically, trabeculotomy showed a success rate of 93.8% (15/16), while filtering surgery exhibited a success rate of 71.8% (28/39). In another study, a series of 38 primary combined trabeculotomy-trabeculectomy procedures and 6 primary trabeculectomy procedures in ARS demonstrated a 93% complete success rate at up to 5 years (2). Furthermore, another study reported the following success rates for ARS: 48% at 5 years for goniotomy, 33% at 15 years for trabeculotomy or combined trabeculotomy and trabeculectomy, and 65% at 10 years for trabeculectomy with antifibrotics (33). The success rate of our study is thus comparable to those reported by other studies. The variations in outcomes across studies may be due to differences in surgical procedures, follow-up duration, and patient-related factors.

The limitations of our study include the sample size of each group being small, owing to the very low incidence of ARS. Our patients were recruited from glaucoma clinics, and most were diagnosed with glaucoma and ARS simultaneously. Therefore, we did not assess the angle features of ARS without glaucoma, and our findings may not apply to all patients with ARS. Finally, since the type of surgery was different among patients, the prognosis of ARS might have been affected.

Conclusions

ARS is a multisystemic developmental disorder, which primarily affects the eyes. Patients are at risk of developing glaucoma throughout their lives, and therefore long-term follow-up is necessary. Our findings provide a basis for classification system of anterior chamber angle dysgenesis *in vivo* and have significant implications for explaining the risk of glaucoma to patients with ARS following UBM

examinations and genetic testing results.

Acknowledgments

The authors are grateful to the Biobank of the Eye, Ear, Nose, and Throat Hospital of Fudan University. The authors would like to thank Youbing Guo, Kailun Lv, Jinling Cao, Aibei Xu, and Bingbing Qu from Amplicon Gene (Shanghai, China) for the helpful bioinformatics analysis. The authors would also like to thank all of the patients and their families.

Funding: This work was supported by the National Natural Science Foundation of China (No. 81870692); the Shanghai Committee of Science and Technology, China (No. 20S31905800); the Clinical Research Plan of SHDC (No. SHDC2020CR6029); the National Key Research and Development Program of China (No. 2020YFA0112700); the State Key Program of National Natural Science Foundation of China (No. 82030027); and the Subject of Major projects of the National Natural Science Foundation of China (No. 81790641).

Footnote

Reporting Checklist: The authors have completed the STROBE reporting checklist. Available at https://qims.amegroups.com/article/view/10.21037/qims-23-348/rc

Conflicts of Interest: All authors have completed the ICMJE uniform disclosure form (available at https://qims.amegroups.com/article/view/10.21037/qims-23-348/coif). The authors have no conflicts of interest to declare.

Ethical Statement: The authors are accountable for all aspects of the work in ensuring that questions related to the accuracy or integrity of any part of the work are appropriately investigated and resolved. The study was conducted in accordance with the Declaration of Helsinki (as revised in 2013) and was approved by the Institutional Review Board of Eye, Ear, Nose, and Throat Hospital of Fudan University (No. KJ2011-04). Written consent forms were obtained from all patients or their legal guardians.

References

1. Kase S, Chin S, Hamanaka T, Shinmei Y, Ohguchi T, Ishida S. Histological observation of trabecular meshwork in a patient with Axenfeld-Rieger syndrome-a new theory for the mechanism of ectropion uvea in congenital glaucoma. Int J Ophthalmol 2020;13:1167-9.
2. Mandal AK, Pehere N. Early-onset glaucoma in Axenfeld-Rieger anomaly: long-term surgical results and visual outcome. Eye (Lond) 2016;30:936-42.
3. Shields MB, Buckley E, Klintworth GK, Thresher R. Axenfeld-Rieger syndrome. A spectrum of developmental disorders. Surv Ophthalmol 1985;29:387-409.
4. Strungaru MH, Dinu I, Walter MA. Genotype-phenotype correlations in Axenfeld-Rieger malformation and glaucoma patients with FOXC1 and PITX2 mutations. Invest Ophthalmol Vis Sci 2007;48:228-37.
5. Shields MB. Axenfeld-Rieger syndrome: a theory of mechanism and distinctions from the iridocorneal endothelial syndrome. Trans Am Ophthalmol Soc 1983;81:736-84.
6. D'haene B, Meire F, Claerhout I, Kroes HY, Plomp A, Arens YH, et al. Expanding the spectrum of FOXC1 and PITX2 mutations and copy number changes in patients with anterior segment malformations. Invest Ophthalmol Vis Sci 2011;52:324-33.
7. Tümer Z, Bach-Holm D. Axenfeld-Rieger syndrome and spectrum of PITX2 and FOXC1 mutations. Eur J Hum Genet 2009;17:1527-39.
8. Zhang Y, Chen X, Wang L, Sun X, Chen Y. Heterogeneity of Axenfeld-Rieger Syndrome: Molecular and Clinical Findings in Chinese Patients. Front Genet 2021;12:732170.
9. Reis LM, Tyler RC, Volkmann Kloss BA, Schilter KF, Levin AV, Lowry RB, Zwijnenburg PJ, Stroh E, Broeckel U, Murray JC, Semina EV. PITX2 and FOXC1 spectrum of mutations in ocular syndromes. Eur J Hum Genet 2012;20:1224-33.
10. Wang X, Liu X, Huang L, Fang S, Jia X, Xiao X, Li S, Guo X. Mutation Survey of Candidate Genes and Genotype-Phenotype Analysis in 20 Southeastern Chinese Patients with Axenfeld-Rieger Syndrome. Curr Eye Res

2018;43:1334-41.
11. Souzeau E, Siggs OM, Zhou T, Galanopoulos A, Hodson T, Taranath D, et al. Glaucoma spectrum and age-related prevalence of individuals with FOXC1 and PITX2 variants. Eur J Hum Genet 2017;25:839-47.
12. Chrystal PW, Walter MA. Aniridia and Axenfeld-Rieger Syndrome: Clinical presentations, molecular genetics and current/emerging therapies. Exp Eye Res 2019;189:107815.
13. Amendt BA, Semina EV, Alward WL. Rieger syndrome: a clinical, molecular, and biochemical analysis. Cell Mol Life Sci 2000;57:1652-66.
14. Tandon A, Watson C, Ayyala R. Ultrasound biomicroscopy measurement of Schlemm's canal in pediatric patients with and without glaucoma. J AAPOS 2017;21:234-7.
15. Hussein TR, Shalaby SM, Elbakary MA, Elseht RM, Gad RE. Ultrasound biomicroscopy as a diagnostic tool in infants with primary congenital glaucoma. Clin Ophthalmol 2014;8:1725-30.
16. Potop V, Coviltir V, Schmitzer S, Dragosloveanu CDM, Ionescu CI, Burcel MG, Corbu MC, Dăscălescu DMC. Ultrasound biomicroscopy in glaucoma assessment. Rom J Ophthalmol 2021;65:114-9.
17. Maslin JS, Barkana Y, Dorairaj SK. Anterior segment imaging in glaucoma: An updated review. Indian J Ophthalmol 2015;63:630-40.
18. Chen WS, Xiang DM, Hu LX. Ultrasound Biomicroscopy Detects Peters' Anomaly and Rieger's Anomaly in Infants. J Ophthalmol 2020;2020:8346981.
19. Guerriero S, L'Abbate M, La Tegola MG, Alessio G, Sborgia G. Combined aniridia ring implantation and cataract surgery in an Axenfeld-Rieger syndrome: a UBM report. Eye Contact Lens 2011;37:45-7.
20. Mannino G, Abdolrahimzadeh B, Calafiore S, Anselmi G, Mannino C, Lambiase A. A review of the role of ultrasound biomicroscopy in glaucoma associated with rare diseases of the anterior segment. Clin Ophthalmol 2016;10:1453-9.
21. Alward WL. Axenfeld-Rieger syndrome in the age of molecular genetics. Am J Ophthalmol 2000;130:107-15.
22. Lines MA, Kozlowski K, Walter MA. Molecular genetics of Axenfeld-Rieger malformations. Hum Mol Genet 2002;11:1177-84.
23. Karaconji T, Zagora S, Grigg JR. Approach to childhood glaucoma: A review. Clin Exp Ophthalmol 2022;50:232-46.
24. Shi Y, Wang H, Han Y, Cao K, Vu V, Hu M, Xin C, Zhang Q, Wang N. Correlation Between Trabeculodysgenesis Assessed by Ultrasound Biomicroscopy and Surgical Outcomes in Primary Congenital Glaucoma. Am J Ophthalmol 2018;196:57-64.
25. Liu J, Li S, Deng G, Yang W, Chen W, Lu H. Ultrasound biomicroscopic imaging in paediatric ocular toxocariasis. Br J Ophthalmol 2017;101:1514-7.
26. Silverman RH. High-resolution ultrasound imaging of the eye - a review. Clin Exp Ophthalmol 2009;37:54-67.
27. Lai I, Mak H, Lai G, Yu M, Lam DS, Leung CK. Anterior chamber angle imaging with swept-source optical coherence tomography: measuring peripheral anterior synechia in glaucoma. Ophthalmology 2013;120:1144-9.
28. Chang TC, Summers CG, Schimmenti LA, Grajewski AL. Axenfeld-Rieger syndrome: new perspectives. Br J Ophthalmol 2012;96:318-22.
29. Michels K, Bohnsack BL. Ophthalmological Manifestations of Axenfeld-Rieger Syndrome: Current Perspectives. Clin Ophthalmol 2023;17:819-28.
30. Gupta V, Jha R, Srinivasan G, Dada T, Sihota R. Ultrasound biomicroscopic characteristics of the anterior segment in primary congenital glaucoma. J AAPOS 2007;11:546-50.
31. Janssens R, van Rijn LJ, Eggink CA, Jansonius NM, Janssen SF. Ultrasound biomicroscopy of the anterior segment in patients with primary congenital glaucoma: a review of the literature. Acta Ophthalmol 2022;100:605-13.
32. Berry FB, Lines MA, Oas JM, Footz T, Underhill DA, Gage PJ, Walter MA. Functional interactions between FOXC1 and PITX2 underlie the sensitivity to FOXC1 gene dose in Axenfeld-Rieger syndrome and anterior segment dysgenesis. Hum Mol Genet 2006;15:905-19.
33. Zepeda EM, Branham K, Moroi SE, Bohnsack BL. Surgical outcomes of Glaucoma associated with Axenfeld-Rieger syndrome. BMC Ophthalmol 2020;20:172.

Cite this article as: Xu Q, Zhang Y, Wang L, Chen X, Sun X, Chen Y. The morphology of angle dysgenesis assessed by ultrasound biomicroscopy and its relationship with glaucoma severity and mutant genes in Axenfeld-Rieger syndrome. Quant Imaging Med Surg 2023;13(10):6979-6988. doi: 10.21037/qims-23-348

Supplementary

Table S1 Comprehensive overview of patients' clinical characteristics, iridocorneal angle morphology, and genetic defects

Patient No.	Sex	Age at first visit	Presenting complaint	Onset age of glaucoma	Iridocorneal angle by number of quadrants (OD)						Corneal clarity (OD)	Iridocorneal angle by number of quadrants (OS)						Corneal clarity (OS)	Mutant gene	Nucleotide changes
					Type A	Type B	Type C	Type D	Type E	Type F		Type A	Type B	Type C	Type D	Type E	Type F			
1	M	1 m	Whitish appearance of the left eye	at birth		1	3				1	1		3				2	FOXC1	c.388C>T
2	M	1 m	Whitish appearance of both eyes	at birth		1.5		2.5			2	-	-	-	-	-	-	2	FOXC1	c.592_593delins C
3	F	1 m	Whitish appearance of both eyes	at birth		4					2		4					2	FOXC1	Gross deletion in 6: 1478641–2694750
4	M	1 m	Whitish appearance of both eyes	at birth		3.5		0.5			2		3.5		0.5			2	FOXC1	c.503_504insGCGGCG
5	M	2 m	Whitish appearance of both eyes	at birth	1.5		2.5				2	1.5		2.5				2	FOXC1	c.392C>T
6	F	9 y	Whitish appearance of both eyes	at birth		3	1				3		3	1				3	FOXC1	c.430A>T
7	M	1 m	Whitish appearance of both eyes	1m		1.5		2.5			2		1.5		2.5			2	FOXC1	c.380G>A
8	M	4 m	Whitish appearance of the right eye	4m			4				2.5	-	-	-	-	-	-	1	FOXC1	c.240_241insTAT
9	M	5 m	Whitish appearance of both eyes	5m		2.5	1.5				2.5		2.5	1.5				2.5	FOXC1	Gross deletion in 6: 382441–2333070
10	M	10 y	Reduced vision in both eyes	10y	1	2.5		0.5			2	1.5	2.5					2	FOXC1	c.275A>C
11	F	14 y	Reduced vision in both eyes	14y		1.5	2.5				1		1	3				1	FOXC1	c.246C>G
12	M	15 y	Reduced vision in both eyes	15y				4			1				4			1	FOXC1	c.482T>A
13	M	15 y	Pain in both eyes	15y		3	1				1		2.5	1.5				1	FOXC1	c.205delC
14	F	18 y	Reduced vision in both eyes	18y		4					1		3.5			0.5		1	FOXC1	c.718_719del
15	F	24 y	Reduced vision in both eyes	24y		3	1				1		3	1				1	FOXC1	c.718_719del
16	F	5 m	Whitish appearance of both eyes	5m					4		2.5					4		2.5	PITX2	c.173T>G
17	M	2 y	Reduced vision in both eyes	2y		1.5			2.5		1		1.5			2.5		1	PITX2	c.348delG
18	F	4 y	Reduced vision in both eyes	4y					3	1	1					3	1	2	PITX2	c.103A>T
19	F	5 y	Reduced vision in both eyes	5y					4		2					4		1	PITX2	c.269G>C
20	F	13 y	Pain in the left eye	13y	-	-	-	-	-	-	1					4		1	PITX2	c.253-11A>G
21	M	17 y	Reduced vision in both eyes	17y						4	1						4	1	PITX2	c.190C>G
22	M	18 y	Reduced vision in both eyes	18y	2.5				1.5		1	3				1		1	PITX2	c.158_173GGTAGCT
23	M	24 y	Reduced vision in the left eye	24y					3	1	1	1				3		1	PITX2	c.253-1G>A
24	M	25 y	Reduced vision in both eyes	25y	3				1		1	3				1		1	PITX2	c.377delC
25	M	30 y	Reduced vision in the left eye	30y	3					1	1	3					1	1	PITX2	c.253-11A>G
26	M	35 y	Reduced vision in both eyes	35y	0.5				3.5		1	0.5	1			2.5		1	PITX2	c.539_551del
27	F	41 y	Pain in both eyes	41y		0.5		0.5	3		2		1.5			2.5		2	PITX2	c.173T>C
28	F	46 y	Pain in both eyes	46y	0.5		0.5		3		2					2.5	1.5	2	PITX2	c.253-11A>G
29	M	61 y	Reduced vision in both eyes	61y	2.5	0.5	0.5			0.5	1	3.5		0.5				1	PITX2	c.282G > A
30	F	10 y	Reduced vision in both eyes	10y	-	-	-	-	-	-	2	0.5	0.5			3		1	/	NA
31	M	14 y	Reduced vision in both eyes	14y	0.5				3.5		1	-	-	-	-	-	-	1	/	NA
32	M	14 y	Reduced vision in both eyes	14y			4				1			4				1	/	NA
33	M	15 y	Reduced vision in both eyes	15y		4					1		4					1	/	NA
34	M	16 y	Pain in both eyes	16y						4	1						4	1	/	NA
35	M	22 y	Reduced vision in both eyes	22y						4	2						4	1	/	NA
36	F	22 y	Pain in both eyes	22y		3	0.5		0.5		1		3	0.5		0.5		1	/	NA
37	M	32 y	Pain in both eyes	32y	3		1				2	3		1				2	/	NA
38	M	34 y	Reduced vision in both eyes	34y	3	1					1	2.5	1.5					1	/	NA
39	F	36 y	Reduced vision in both eyes	36y	1				0.5	2.5	1	1				0.5	2.5	1	/	NA
40	F	36 y	Pain in both eyes	36y	1				3		1	-	-	-	-	-	-	1	/	NA
41	F	42 y	Reduced vision in the right eye	42y		3	0.5	0.5			1		3	1				1	/	NA
42	M	70 y	Reduced vision in both eyes	70y	3	1					2	3	1					1	/	NA

Type A: pure high iris insertion; Type B: posterior embryotoxon; Type C: iris process; Type D: trabecular-iris synechia; Type E: peripheral iridocorneal adhesion; Type F: goniodysgenesis. No. 14 and No. 15 are sisters; No. 25 is the father of No. 20. OD, right eye; OS, left eye; M, male; F, female; -, excluded in this study; /, negative for the variant; NA, not applicable.

https://dx.doi.org/10.21037/qims-23-348